Supplementary materials for

Morphological and mechanical determinants of cellular uptake of deformable nanoparticles

Liping Chen[†], Xuejin Li[‡], Yunhan Zhang[†], Tongwei Chen[†], Shiyan Xiao[†,*], Haojun Liang[†,¶,*]

† CAS Key Laboratory of Soft Matter Chemistry, iChEM (Collaborative Innovation Center of Chemistry for Energy Materials), Department of Polymer Science and Engineering, University of Science and Technology of China, Hefei, Anhui 230026, P. R. China.

‡ Department of Engineering Mechanics and Key Laboratory of Soft Machines and Smart Devices of Zhejiang Province, Zhejiang University, Hangzhou 310027, P. R. China

¶ Hefei National Laboratory for Physical Sciences at the Microscale, University of Science and Technology of China, Hefei, Anhui 230026, P. R. China.

*To whom correspondence should be addressed. E-mail: xiaosy@ustc.edu.cn (S. X.), or hljiang@ustc.edu.cn (H. L.).

Methods of free energy calculations for NP endocytosis

To understand the effect of the elasticity of a NP on its endocytosis, we calculate the change in free energy as a function of the distance between the particle center and the bilayer midplane by the way of constrained thermodynamic integration (TI).

To determine the free energy change of a NP as it is uptaken by bilayer, we adopt a parameter λ to measure the normalized distance from the NP center to the midplane of membrane as

$$z(\lambda) = z(\lambda = 0) + \lambda[z(\lambda = 1) - z(\lambda = 0)] \text{ .}$$

(1)

Here, λ is set to 0 when the NP stands at an initial position above the lipid bilayer. As membrane wraps the NP, λ gradually increase and finally reaches 1 when the NP is wholly wrapped. The free energy change in this process is expressed as:

$$\Delta F = \int_0^{\lambda} \frac{\partial F(\lambda)}{\partial \lambda} d\lambda \text{ ,}$$

(2)

According to eqn (2), we discretize the NP uptake path by choosing a series of λ values between 0 and 1. For each chosen value of λ, a harmonic potential

$$U(\lambda) = \frac{k_Z}{2}[Z - z(\lambda)]^2$$

(3)

is imposed to confine the motion of the NP in the z-direction, where $k_z = 300$ and $z(\lambda)$ are the spring constant and equilibrium position of the potential, respectively; Z is the position of the NP center. Under the harmonic constraint, the NP is forced to oscillate around a pseudo-equilibrium position $\langle Z \rangle$ in the vicinity of $z(\lambda)$, where $\langle Z \rangle$ is the ensemble-averaged position of the NP center. The derivative of the free energy is determined from the constrained interaction between the NP and surrounding as

$$\frac{\partial F(\lambda)}{\partial \lambda} = \left\langle \frac{\partial U(\lambda)}{\partial \lambda} \right\rangle.$$

(4)

The integrand of eqn (4) is thus obtained from the simulated value of $\langle Z \rangle$ as:

$$\frac{\partial F(\lambda)}{\partial \lambda} = k_z[\langle Z\rangle - z(\lambda)]\, z(\lambda = 0).$$

(5)

Integration this expression allows the free energy change to be determined as a function of distance from the bilayer midplane,

$$\Delta F = \int_{z(\lambda = 0)}^{z(\lambda = \varepsilon)} k_z[z(\lambda) - \langle Z\rangle] dz, \quad (0 \le \varepsilon \le 1).$$

(6)

Based on equation (6), we calculated the PMF profiles of the endocytic process for NPs as a function of the distance between the particle center and the membrane midplane, as displayed in Fig. 8 in the main text.

Mechanical properties for model membrane

The bending rigidity of a flat membrane can be derived using thermal fluctuation spectrum of a membrane[1-3].

A symmetric flat membrane can be modeled as a two-dimensional curvature-elastic surface. The energy of a deformed piece of membrane is given by the classical Helfrich Hamiltonian[4,5] as following,

$$E_{bend} = \frac{1}{2}\int dxdy[\kappa(\Delta h)^2 + \Sigma(\Delta h)^2] \tag{7}$$

Where κ and Σ are the bending modulus and lateral surface tension, respectively. $h(x,y)$ is the membrane shape, represented using the height of the membrane above the same reference plane. For a membrane with a quadratic frame of size $L \times L$, we can expand the bilayer shape in modes $h(r) = \sum_q h_q e^{iq \cdot r}$, with $q = 2\pi/L(n_x,n_y)$, $n_x,n_y \in Z$. Equation (7) can be rewritten as,

$$E_{bend} = L^2 \sum_q |h_q|^2 \left\{\frac{1}{2}\kappa q^4 + \frac{1}{2}\Sigma q^2\right\} \tag{8}$$

From the equipartition theorem, we have,

$$\frac{1}{2}k_B T = L^2 |h_q|^2 \left\{\frac{1}{2}\kappa q^4 + \frac{1}{2}\Sigma q^2\right\} \tag{9}$$

We therefore can immediately give,

$$\langle |h_q|^2 \rangle = \frac{k_B T}{L^2[\kappa q^4 + \Sigma q^2]} \tag{10}$$

Measuring the spectrum of thermal fluctuation of membrane, and fitting it to equation (10) gives the bending modulus κ and lateral tension Σ. Obviously, for a membrane with zero tension, $\langle |h_q|^2 \rangle$ scales linearly with q^4.

To measure the bending modulus of our modeled membranes, a flat square membrane spanning in the x-y plane is built using a total of 7200 lipids. Periodic boundary conditions (PBCs) have been used to obtain an infinite membrane in the liquid phase. Throughout the simulation of each modeled

system, the box lengths in x and y dimensions of the membrane-spanning domain were varied to achieve a zero external pressure, while the height of the box remained constant. The temperature is set to $T = 1.1\epsilon/k_B$, the time step is set to 0.005τ. The built systems are first relaxed for $20000\,\tau$ (4×10^6 steps), followed by an equilibrium simulation of $30000\,\tau$ (6×10^6 steps) for fluctuation analyses. For each simulated system, the trajectory is saved every 300 steps, a total of 20000 frames are used for fluctuation calculations.

The membrane is divided into a 32×32 grid, the length of each patch is $l = L/32$. For each frame of the simulation trajectory, the displacements of each lipid head from the reference plane in each patch is averaged to calculate the membrane shape $h(r)$, $r = (x, y)$. The derived $h(r)$ is expanded in Fourier modes using python program. The bending modulus is obtained by fitting h_q to equation (10), see figure S6(a).

To study the mechanical properties of membrane with different value of α_m, five systems of free membrane are constructed by setting α_m equals 1.00, 1.02, 1.04, 1.06, 1.08. The measured values of bending modulus (κ) are depicted as a function of α_m in figure S6(b).

The effects of global area constraint to the uptake kinetics.

To examine the effects of global area constraint to the uptake kinetics, we studied the uptake kinetics of elastic NP with varied k_a, taking the sphere as an example. The volume of the simulated sphere is set to $533\pi\sigma^3$. (Fig. 10)

It is found that the enhancement of global area constraint (k_a changed from $1\ \epsilon\sigma^{-2}$ to $100\ \epsilon\sigma^{-2}$) affects negligibly to the uptake kinetics for the sphere.

After that, a more flexible spherical NP ($k_s = 20\ \epsilon\sigma^{-2}$, $k_b = 0.5\ \epsilon$, $k_v = 10\ \epsilon\sigma^{-2}$) was tested to study the effects of global area constraint to the uptake kinetics. It is observed that the uptake kinetics differs very slightly.

Based on the above calculations, it is concluded that the global area constraint plays a less important role in regulating the uptake kinetics, in comparison with the bond and bending constraints.

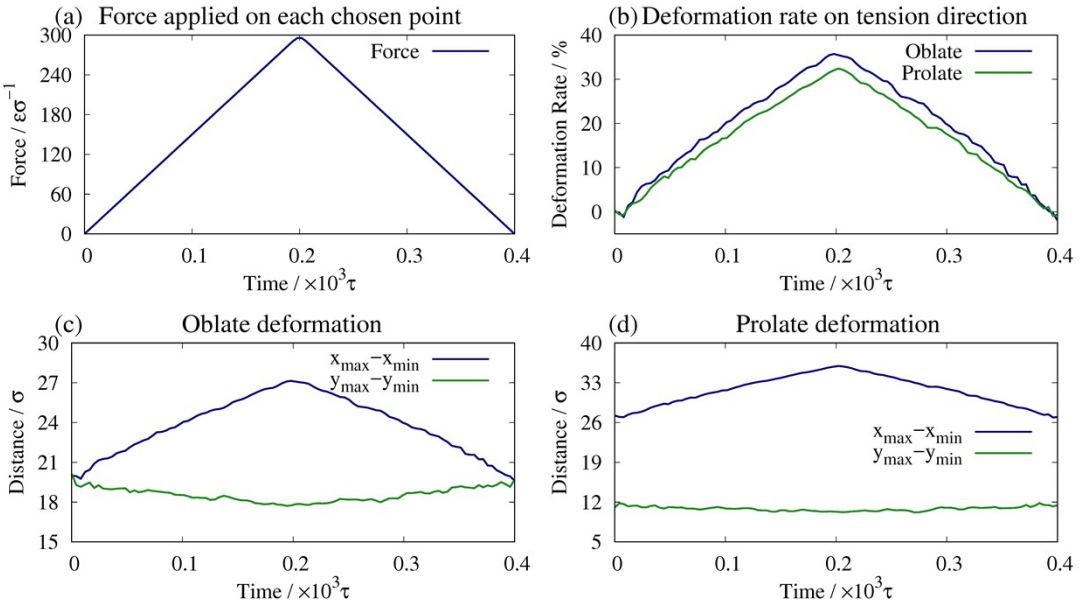

Figure S1 Stretching forces are applied to the prolate or oblate NP to examine their elastic behaviors, with the force versus simulation time recorded in (a), and the axial in x-dimension and transverse diameters in y- and z-dimensions shown in (b-d).

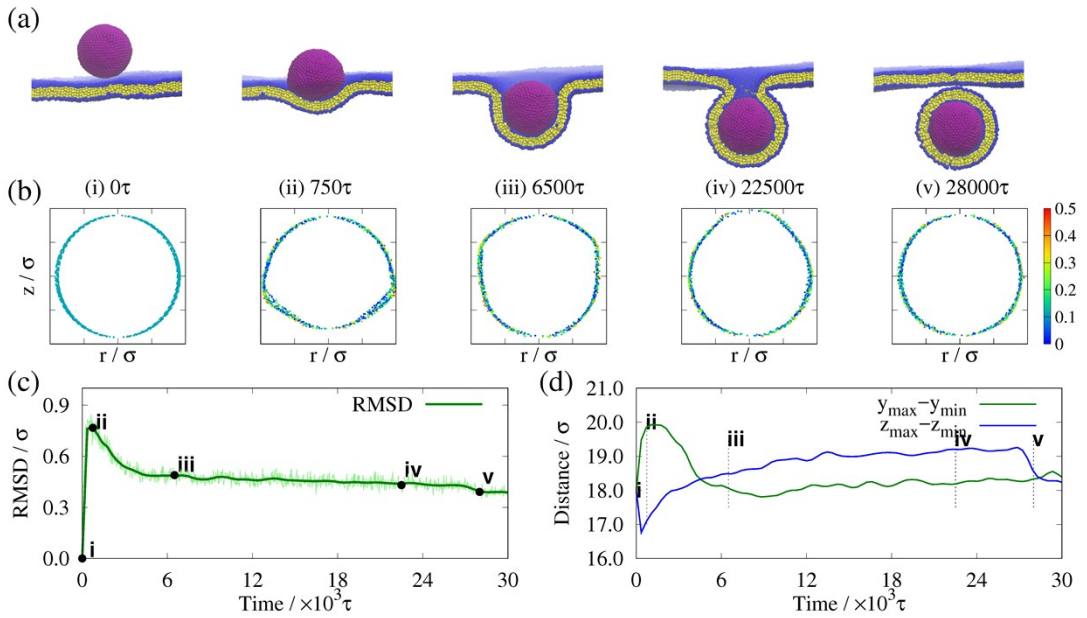

Figure S2 Endocytic process of elastic spherical NP with a volume of $972\pi\sigma^3$, the radius of which is 9σ. The parameter of membrane rigidity α_m is set to 1.04, the strength of membrane-NP interactions α_{LJ} is set to 1.3. (a) Representative snapshots of the internalization pathway of elastic spherical NP, the contour line of NP in each snapshot is shown in (b), with the color denoting the value of mean curvature. Time evolutions of root-mean-squared-deviation (RMSD) and the transverse diameters in the y and z dimensions are shown in (c) and (d), respectively.

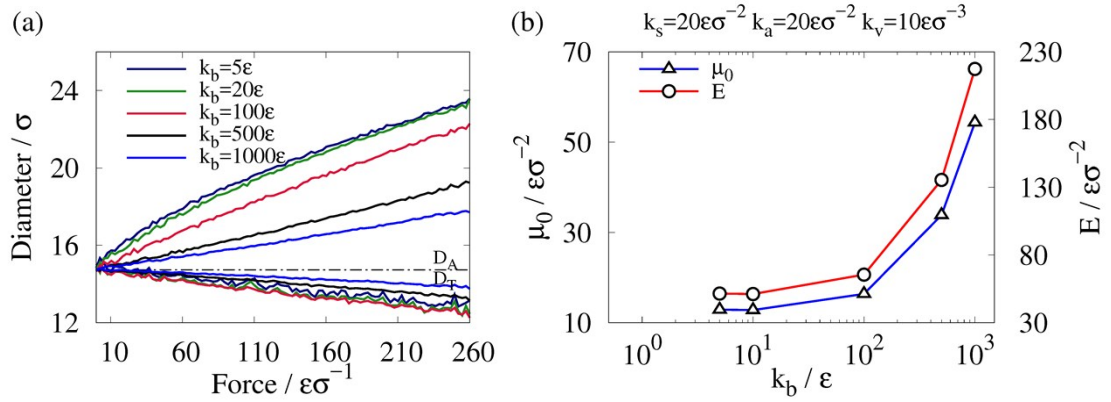

Figure S3 Stretching response simulations of elastic sphere with varied bending modulus k_b. The volume of sphere is $533\pi\sigma^3$. (a) Axial and transverse diameters (D_A and D_T) of the elastic sphere versus the total stretching force. The parameters used for spherical NP: $k_s = 20\ \epsilon\sigma^{-2}$, $k_a = 20\ \epsilon\sigma^{-2}$, $k_v = 10\ \epsilon\sigma^{-3}$. Five elastic spherical NPs with varied values of bending modulus have been tested, that is, k_b was set to $5\ \epsilon$, $20\ \epsilon$, $100\ \epsilon$, $500\ \epsilon$, and $1000\ \epsilon$. (b) The initial in-plane shear modulus (μ_0) and Young's modulus versus the bending modulus (k_b).

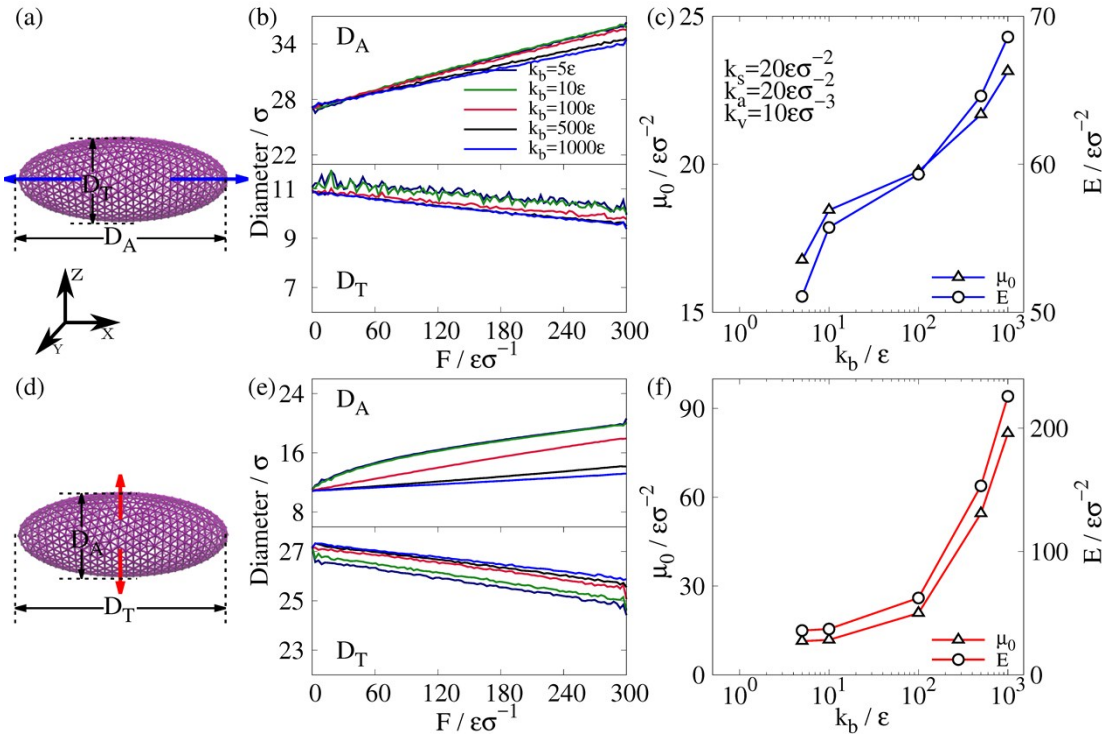

Figure S4 Stretching response simulations of elastic prolate with varied bending modulus k_b. The volume of prolate is $533\pi\sigma^3$. Stretching force is applied to the prolate in x-direction (a-c), and z-direction (d-f) in order to test the anisotropy of elasticity. (b) and (e) depict the axial and transverse diameters (D_A and D_T) versus the total stretching force. (c) and (f) depict the initial in-plane shear modulus (μ_0) and Young's moduli versus the bending modulus (k_b). For these simulations, $k_s = 20\,\epsilon\sigma^{-2}$, $k_a = 20\,\epsilon\sigma^{-2}$, $k_v = 10\,\epsilon\sigma^{-3}$. Five elastic prolate NPs with varied values of bending modulus have been tested, that is, k_b was set to $5\,\epsilon$, $20\,\epsilon$, $100\,\epsilon$, $500\,\epsilon$, and $1000\,\epsilon$.

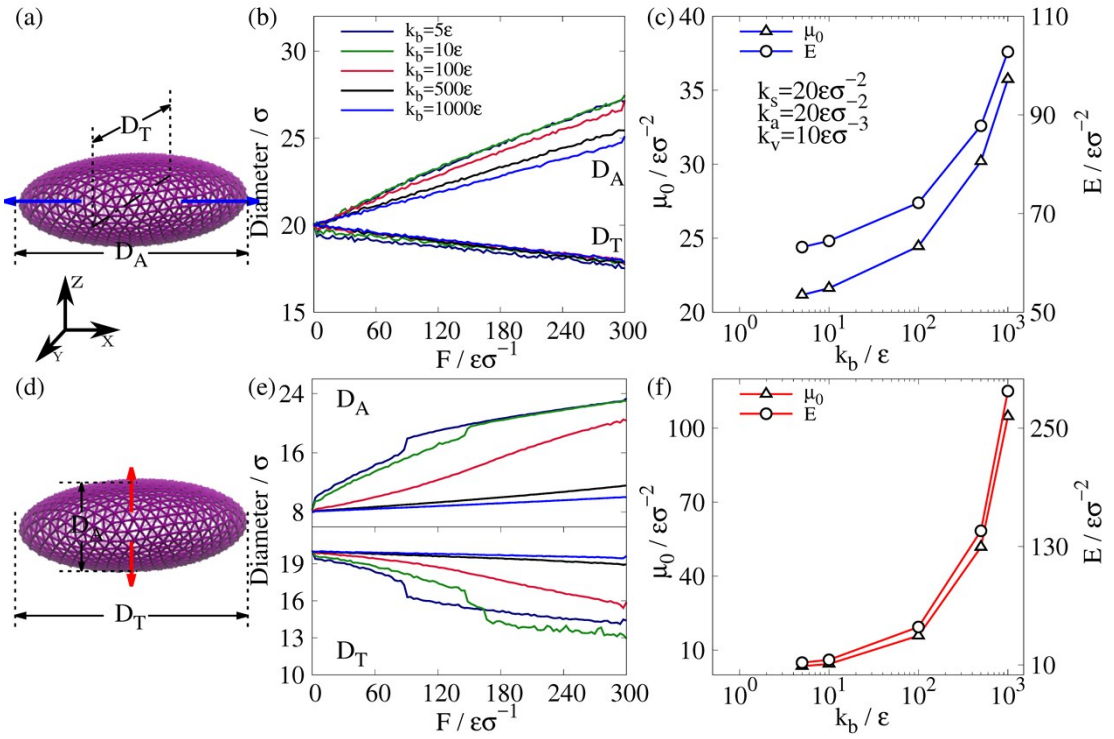

Figure S5 Stretching response simulations of elastic oblate with varied bending modulus k_b. The volume of oblate is $533\pi\sigma^3$. Stretching force is applied to the prolate in x-direction (a-c), and y-direction (d-f) in order to test the anisotropy of elasticity. (b) and (e) depict the axial and transverse diameters (D_A and D_T) versus the total stretching force. (c) and (f) depict the initial in-plane shear modulus (μ_0) and Young's moduli (E) versus the bending modulus (k_b). For these simulations, $k_s = 20\,\epsilon\sigma^{-2}$, $k_a = 20\,\epsilon\sigma^{-2}$, $k_v = 10\,\epsilon\sigma^{-3}$. Five elastic oblate NPs with varied values of bending modulus have been tested, that is, k_b was set to $5\,\epsilon$, $20\,\epsilon$, $100\,\epsilon$, $500\,\epsilon$, and $1000\,\epsilon$.

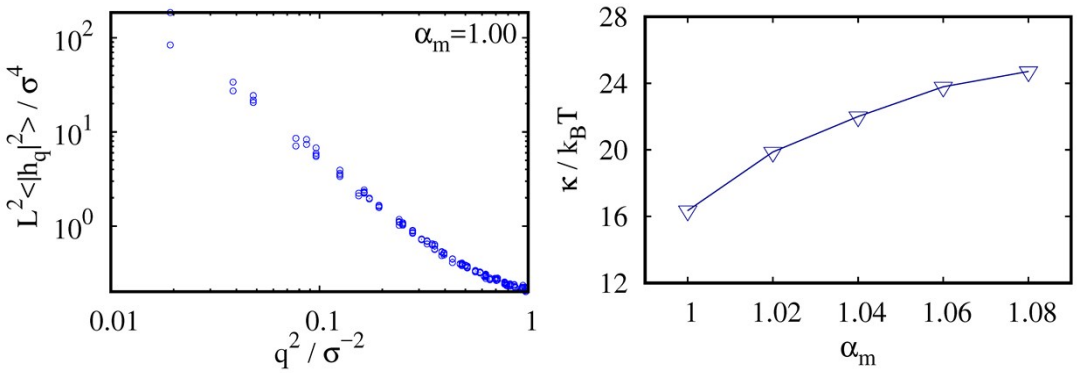

Figure S6 (a) The power spectrum $\langle |h_q|^2 \rangle$ for the bilayer system with $\alpha_m = 1.00$. (b) The relation between membrane bending modulus (κ) with α_m.

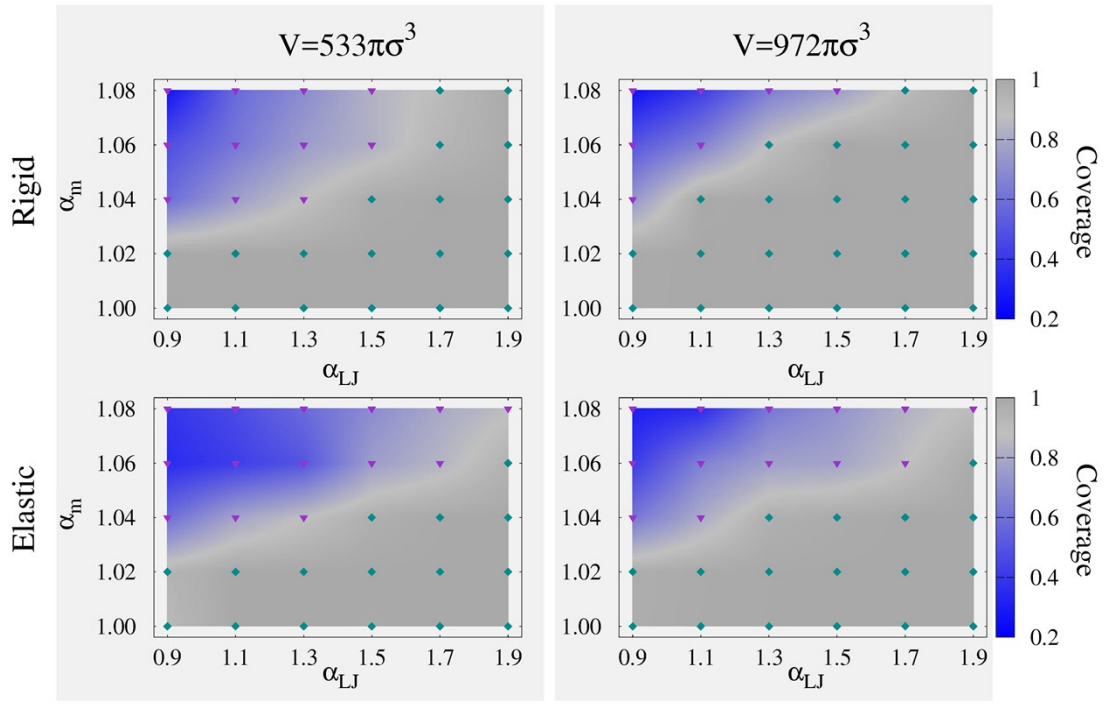

Figure S7 To study the effects of volume and membrane rigidity on the behaviors of elastic sphere internalization, the phase diagram for the final states of rigid and elastic spherical NPs with a volume of $972\pi\sigma^3$ being wrapped by bilayer (shown in the right row). Note that the phase diagram for the sphere with a volume of $533\pi\sigma^3$ is depicted again for direct comparison. The final states are represented using symbols: ▼ partially wrapped structure, ♦ wrapped structure.

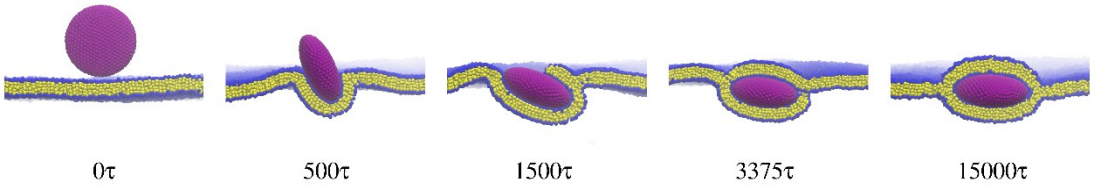

Figure S8 Sequential snapshots for process of the formation of sandwiched superstructure of elastic oblate NP incorporated by membrane. The volume of oblate is $533\pi\sigma^3$. The membrane rigidity α_m is set to 1.02, the strength of membrane-NP interactions α_{LJ} is set to 1.9.

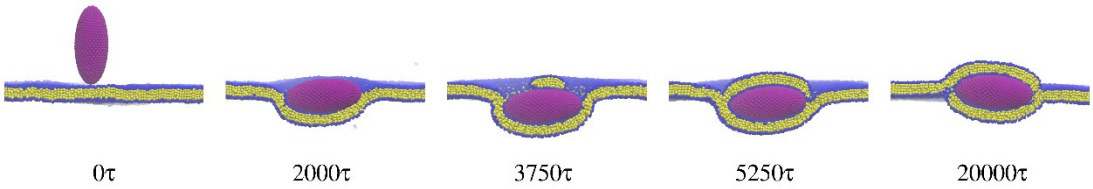

Figure S9 Sequential snapshots for process of the formation of sandwiched superstructure of elastic prolate NP incorporated by membrane. The volume of prolate is $533\pi\sigma^3$. The membrane rigidity α_m is set to 1.02, the strength of membrane-NP interactions α_{LJ} is set to 1.9.

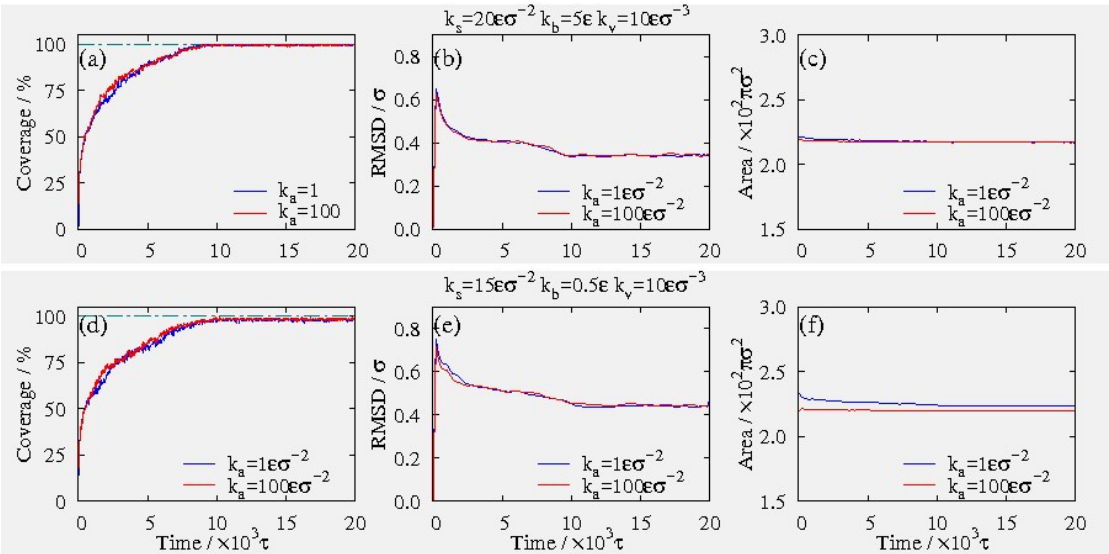

Figure S10 The uptake behaviors for the sphere, with varied constraint constants for the global surface area constraint. Time evolutions of coverage percentage (left), RMSD (middle) and surface area (right) as a function of simulation time are depicted. The volume of the sphere is $533\pi\sigma^3$. Upper panel: $k_s = 20\ \epsilon\sigma^{-2}$, $k_b = 5\ \epsilon$, $k_v = 10\ \epsilon\sigma^{-2}$; lower panel: $k_s = 20\ \epsilon\sigma^{-2}$, $k_b = 0.5\ \epsilon$, $k_v = 10\ \epsilon\sigma^{-2}$.

Two values of k_a are tested herein: $k_a = 1\ \epsilon\sigma^{-2}$, and $k_a = 100\ \epsilon\sigma^{-2}$.

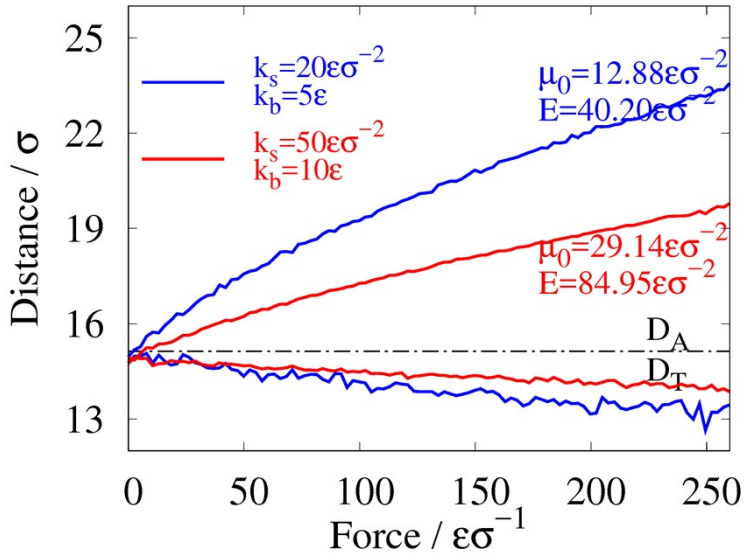

Figure S11 Stretching response simulation for the sphere with varied elasticity. Axial and transverse diameters (D_A and D_T) of the elastic sphere versus stretching force are depicted. The stiffness of sphere is modulated using k_s and k_b. The more rigid sphere setup: $k_s = 50\ \epsilon\sigma^{-2}$, $k_b = 10\ \epsilon$, marked in red in the figure; The less rigid sphere setup: $k_s = 20\ \epsilon\sigma^{-2}$, $k_b = 5\ \epsilon$, marked in blue in the figure.

For the simulations herein, $k_a = 20\,\epsilon\sigma^{-2}$, $k_v = 10\,\epsilon\sigma^{-3}$. The calculated initial in-plane shear modulus (μ_0) and Young's moduli (E) are depicted in the figure.

Table S1 Simulation parameters used in the present work.

	$k_s\,(\epsilon\sigma^{-2})$	$k_b\,(\epsilon)$	$k_a\,(\epsilon\sigma^{-2})$	$k_v\,(\epsilon\sigma^{-3})$
Sphere	20.0	5.0	20.0	10.0
Oblate	20.0	5.0	20.0	10.0
Prolate	20.0	5.0	20.0	10.0

References

(1) Cooke, I. R.; Deserno, M. *J. Chem. Phys.* **2005**, *123*, 224710.
(2) Cooke, I. R.; Kremer, K.; Deserno, M. *Phys. Rev. E* **2005**, *72*, 011506.
(3) Deserno, M. *Macromol. Rapid Commun.* **2009**, *30*, 752.
(4) Canham, P. B. *Journal of Theoretical Biology* **1970**, *26*, 61.
(5) Helfrich, W. *Z Naturforsch C.* **1973**, *28*, 693.